Debye Representation of Frequency Dependent Ground for LEMP Analysis With RC-FDTD

Osman Kurnaz and Serkan Aksoy

***Abstract*—Finite-difference time-domain (FDTD) method combined with the recursive convolution technique is applied to compute lightning electromagnetic pulses (LEMP) for dispersive ground adopting Longmire and Smith (LS) model in two-dimensional cylindrical coordinates. The novelty of our study is that, to the best of our knowledge, the LEMP simulation has been realized in the time-domain for the first time by directly using the parameters of the LS dispersive soil model by treating the ground as a multipole Debye medium without using approximate techniques such as vector fitting. As a numerical example, the LEMP is simulated above and under the dispersive ground with buried rock formation, which is also modeled as the dispersive Debye medium. The performed simulations are compared at distances of 500 m, 5 km, and 50 km away from the lightning channel for both first stroke and subsequent stroke. The results show that the case of dispersive ground and the rock leads to a difference of up to 61.77% with respect to using constant electrical parameters.**

***Index Terms*—Debye model, dispersive (frequency-dependent) ground, finite-difference time-domain (FDTD), lightning, Longmire and Smith (LS) model, recursive convolution (RC).**

I. Introduction

In THE analysis of lightning electromagnetic pulses (LEMP), the finite-difference time-domain (FDTD) method [1] is very popular due to its advantages [2]. Nevertheless, the studies adopting the FDTD generally use constant electrical parameters for the ground. Several dispersive (frequency-dependent) soil models are defined in the literature [3]. Moreover, very huge errors exceeding 100% are reported to introduce if constant parameters are used instead of dispersive ground models in the LEMP problems [4]. For more realistic LEMP simulations, the researchers use frequency domain methods and convert the results to time-domain applying Fourier or Laplace transformations [5], [6], [7], [8], [9], [10], [11], [12], [13], [14], [15], [16], [17], [18], [19]. However, such an indirect approach may introduce spurious information due to bandwidth or time step restrictions [20]. Also, these techniques require computations at several frequencies [17], [21]. For this reason, the direct time-domain methods are demanded [22], [23], [24], [25], [26]. On the other hand, most of these studies use some approximate techniques like vector fitting for the frequency dependence of the soil model.

Leaving aside the other methods, the first lightning-related FDTD paper modeling the dispersive ground (not the LS model) as the multipole Debye model is published by Kuklin in 2016 [27]. He used the auxiliary differential equation (ADE) for dispersive calculations and extended thin wire techniques to calculate grounding potential rise. In that study, good approximation is possible if resistivity is close to certain value. In 2017, Oliveira et al. approximated the soil parameters with Pade coefficients and used the ADE in the FDTD [28]. They computed lightning induced voltages and compared the results with their own measurements. In their algorithm, the use of high-precision variables is necessary to avoid numerical divergence. Moreover, complex-numbered electric fields must be stored and updated. All these need computer RAM. In 2018, Sun et al. used the FDTD method to evaluate underground LEMP and took soil dispersion into account adopting a semi-analytical recursive convolution (SARC) algorithm [29]. They approximated the soil parameters using vector-fitting scheme and compared their results with Cooray-Rubinstein formula. In 2021, Rizk et al. computed lightning-induced voltages on overhead lines due to nearby first and subsequent return strokes using the method of FDTD [30]. They included the frequency-dependence of the ground utilizing vector-fitting and recursive convolution (RC). The common drawback of all these papers is that they use approximations to represent dispersive soil parameters in their proposed models instead of the exact dispersive soil models.

In this article, the two-dimensional (2-D) FDTD method combined with the RC technique is used to solve the LEMP problem for the dispersive soil. The advantage of our study is that it contains no approximation and utilizes the LS model directly in the FDTD equations by treating the ground as a multipole Debye medium, which can be considered as a novel application of the LEMP computation with the FDTD method. This article is organized as follows: In Section I, a background on the topic is provided. In Section II, theoretical details are presented with the validation of the used method. A numerical example at both near and far range distances can be found in Section III, and Section IV presents the concluding ideas.

Manuscript received 15 January 2022; revised 16 May 2022; accepted 8 June 2022. Date of publication 22 September 2022; date of current version 14 December 2022. This work was supported by The Scientific and Technological Research Council of Turkey under Grant 122E327. *(Corresponding author: Serkan Aksoy.)*

The authors are with the Department of Electronics Engineering, Gebze Technical University, Gebze 41400, Turkey (e-mail: osmankurnaz@gtu.edu.tr; saksoy@gtu.edu.tr).

Color versions of one or more figures in this article are available at https://doi.org/10.1109/TEMC.2022.3206412.

Digital Object Identifier 10.1109/TEMC.2022.3206412

TABLE I
a_q COEFFICIENTS

q	1	2	3	4	5	6	7
a_q	3.4×10^6	2.74×10^5	2.58×10^4	3.38×10^3	5.26×10^2	1.33×10^2	2.72×10^1
q	8	9	10	11	12	13	
a_q	1.25×10^1	4.8×10^0	2.17×10^0	9.8×10^{-1}	3.92×10^{-1}	1.73×10^{-1}	

II. THEORETICAL APPROACH

A. Conversion of the LS Soil Parameters to Debye Model

In our analysis, we adopted the dispersive soil model proposed by Longmire and Smith [31], which was adopted in [14], [15], [16], [17], and [29] previously. According to the Longmire and Smith (LS) model, relative permittivity (ε_r) and conductivity (σ) of the dispersive soil are expressed as follows:

$$\varepsilon_r(f) = \varepsilon_\infty + \sum_{q=1}^{13} \frac{a_q}{1 + (f/F_q)^2} \tag{1a}$$

$$\sigma(f) = \sigma_0 + 2\pi\varepsilon_0 \sum_{q=1}^{13} a_q F_q \frac{(f/F_q)^2}{1 + (f/F_q)^2} \ (\mathrm{S/m}) \tag{1b}$$

$$\varepsilon_\infty = 5, \ \ \sigma_0 = \ 8 \times 10^{-3} \times (p/10)^{1.54} \ (\mathrm{S/m}) \tag{1c}$$

$$F_q = (p/10)^{1.28} \ \times 10^{q-1} \tag{1d}$$

where σ_0 is low-frequency conductivity, ε_0 is permittivity of the free space, f is frequency ranging from dc to 5 MHz, p is soil water percentage, and a_q is a coefficient presented in Table I. For the LS model, the frequency variations of the conductivity and permittivity are given in [29]. Evaluating the frequency spectrums of our graphical results, it can be concluded that their frequency spectrums well correspond to the frequency band of the conductivity and permittivity variations in the LS model. According to [29], it is also clear that the conductivity is near constant at low frequencies and is increasing with frequency while the permittivity is significantly decreasing with frequency. It means that the conductivity is more influential at high frequencies while the permittivity is influential at low frequencies.

In general, the frequency-dependent effective complex relative permittivity of the ground can be defined as [3]

$$\varepsilon_{eff}(f) \ = \varepsilon_r \ (f) - j\frac{\sigma(f)}{\omega\varepsilon_0} \tag{2}$$

where $\omega \ = \ 2\pi f$. Using the notation ω instead of f , we can get

$$\varepsilon_{eff}(\omega) \ = \varepsilon_\infty - j\frac{\sigma_0}{\omega\varepsilon_0} + \sum_{q=1}^{13} \left(\frac{a_q}{1 + \left(\frac{\omega}{2\pi F_q}\right)^2} - j\frac{\left(\frac{a_q}{2\pi F_q}\right)\omega}{1 + \left(\frac{\omega}{2\pi F_q}\right)^2} \right) \tag{3a}$$

and it is simplified to

$$\varepsilon_{eff}(\omega) = \varepsilon_\infty + \frac{\sigma_0}{j\omega\varepsilon_0} + \sum_{q=1}^{13} \frac{a_q}{1 + j\frac{\omega}{2\pi F_q}} \tag{3b}$$

where (3a) is obtained by substituting the LS parameters into (2). The conversion of (3a)–(3b) is straightforward since the summation term in (3b) is nothing but just the combination of real and imaginary parts of the summation term in (3a). The first two terms in (3b) already exist in the lossy case. The term inside the summation is observed to be in the form of multipole Debye model [32] with modified parameters and represents the dispersive part. Then, we can define the electrical susceptibility $\chi(\omega)$ and its inverse Fourier transform $\chi(t)$ as a multi-pole Debye model

$$\chi(\omega) = \sum_{q=1}^{13} \frac{a_q}{1 + j\frac{\omega}{2\pi F_q}} \tag{4a}$$

$$\chi(t) = \sum_{q=1}^{13} \left[a_q (2\pi F_q) e^{-(2\pi F_q)t} u(t) \right] \tag{4b}$$

where $u(t)$ is the unit step function.

B. FDTD Update Equations

In 2-D cylindrical coordinates and assuming $\mathrm{TM_z}$ mode, Maxwell's equations in linear isotropic dispersive media are as

$$\frac{\partial D_r}{\partial t} = \ -\sigma_0 E_r - \frac{\partial H_\varphi}{\partial z} \tag{5a}$$

$$\frac{\partial D_z}{\partial t} = \ -\sigma_0 E_z + \frac{1}{r}\frac{\partial (r H_\varphi)}{\partial r} \tag{5b}$$

$$\frac{\partial H_\varphi}{\partial t} = \frac{1}{\mu}\left[\frac{\partial E_z}{\partial r} - \frac{\partial E_r}{\partial z} \right] \tag{5c}$$

where

$$\vec{D}(\omega) = \varepsilon_0 [\varepsilon_\infty + \chi(\omega)] \vec{E}(\omega) \tag{6a}$$

$$\vec{D}(t) = \varepsilon_0 \varepsilon_\infty \vec{E}(t) + \varepsilon_0 \int_0^t \vec{E}(t-\tau)\chi(\tau)\, d\tau. \tag{6b}$$

We can discretize (5a) as

$$\frac{D_r\Big|_{i+\frac{1}{2},j}^{n+1} - D_r\Big|_{i+\frac{1}{2},j}^{n}}{\Delta t} = -\sigma_0 E_r\Big|_{i+\frac{1}{2},j}^{n+1} - \frac{H_\varphi\Big|_{i+\frac{1}{2},j+\frac{1}{2}}^{n+\frac{1}{2}} - H_\varphi\Big|_{i+\frac{1}{2},j-\frac{1}{2}}^{n+\frac{1}{2}}}{\Delta z} \tag{7}$$

and by following the procedure in [33] and [34], we can write

$$D_r\Big|_{i+\frac{1}{2},j}^{n+1} = \varepsilon_0\varepsilon_\infty \, E_r\Big|_{i+\frac{1}{2},j}^{n+1} + \varepsilon_0 \sum_{m=0}^{n} E_r\Big|_{i+\frac{1}{2},j}^{n+1-m} \int_{m\Delta t}^{(m+1)\Delta t} \chi(\tau)\, d\tau \tag{8a}$$

$$D_r\Big|_{i+\frac{1}{2},j}^{n} = \varepsilon_0\varepsilon_\infty E_r\Big|_{i+\frac{1}{2},j}^{n} + \varepsilon_0 \sum_{m=0}^{n-1} E_r\Big|_{i+\frac{1}{2},j}^{n-m} \int_{m\Delta t}^{(m+1)\Delta t} \chi(\tau)\, d\tau. \tag{8b}$$

To simplify, we define

$$\chi_m = \int_{m\Delta t}^{(m+1)\Delta t} \chi(\tau)\, d\tau; \;\; \Delta\chi_m = \chi_m \; - \chi_{m+1}. \tag{9}$$

Then, we can write

$$D_r\Big|_{i+\frac{1}{2},j}^{n+1} - D_r\Big|_{i+\frac{1}{2},j}^{n} = \varepsilon_0 \;(\varepsilon_\infty + \chi_0)\, E_r\Big|_{i+\frac{1}{2},j}^{n+1} - \varepsilon_0\varepsilon_\infty E_r\Big|_{i+\frac{1}{2},j}^{n} - \varepsilon_0 \sum_{m\,=\,0}^{n-1} E_r\Big|_{i+\frac{1}{2},j}^{n-m} \Delta\chi_m. \tag{10}$$

We defined ψ_r

$$\psi_r\Big|_{i+\frac{1}{2},j}^{n} = \sum_{m=0}^{n-1} E_r\Big|_{i+\frac{1}{2},j}^{n-m} \Delta\chi_m \tag{11}$$

and implemented the RC technique to the multiterm LS model. The details of the implementation steps of the RC technique are clearly described in the Appendix of [33] for the single-pole Debye medium. Since the terms in the summation part of the LS model are independent from each other, we can end up with the following:

$$\psi_r\Big|_{i+\frac{1}{2},j}^{n} = E_r\Big|_{i+\frac{1}{2},j}^{n} \Delta\chi_0 + \sum_{q\,=\,1}^{13} \left[\left(e^{-(2\pi F_q)\Delta t}\right) \psi_{r,q}\Big|_{i+\frac{1}{2},j}^{n-1}\right] \tag{12}$$

where $\Delta\chi_0$ can be found by evaluating the expressions in (9) as

$$\Delta\,\chi_0 = \sum_{q=1}^{13} a_q \left[\left(1 - e^{-(2\pi F_q)\Delta t}\right)^2\right]. \tag{13}$$

We can express (12) in a better way by demonstrating it in a vector form as

$$\psi_r\Big|_{i+\frac{1}{2},j}^{n} = \psi_{r,1}\Big|_{i+\frac{1}{2},j}^{n} + \psi_{r,2}\Big|_{i+\frac{1}{2},j}^{n} + \cdots + \psi_{r,13}\Big|_{i+\frac{1}{2},j}^{n} \tag{14a}$$

$$\begin{pmatrix} \psi_{r,1}\Big|_{i+\frac{1}{2},j}^{n} \\ \psi_{r,2}\Big|_{i+\frac{1}{2},j}^{n} \\ \vdots \\ \psi_{r,13}\Big|_{i+\frac{1}{2},j}^{n} \end{pmatrix} = E_r\Big|_{i+\frac{1}{2},j}^{n} \begin{pmatrix} a_1\left(1 - e^{-(2\pi F_1)\Delta t}\right)^2 \\ a_2\left(1 - e^{-(2\pi F_2)\Delta t}\right)^2 \\ \vdots \\ a_{13}\left(1 - e^{-(2\pi F_{13})\Delta t}\right)^2 \end{pmatrix} + \begin{pmatrix} e^{-(2\pi F_1)\Delta t} \\ e^{-(2\pi F_2)\Delta t} \\ \vdots \\ e^{-(2\pi F_{13})\Delta t} \end{pmatrix} \cdot \begin{pmatrix} \psi_{r,1}\Big|_{i+\frac{1}{2},j}^{n-1} \\ \psi_{r,2}\Big|_{i+\frac{1}{2},j}^{n-1} \\ \vdots \\ \psi_{r,13}\Big|_{i+\frac{1}{2},j}^{n-1} \end{pmatrix}. \tag{14b}$$

After combining (7), (10), and (11), and following [35], [36], we can obtain the update equation for E_r as

$$E_r\Big|_{i+\frac{1}{2},j}^{n+1} = \frac{1}{\varepsilon_\infty + \chi_0 + \frac{\sigma_0\Delta t}{\varepsilon_0}} \times \left[\varepsilon_\infty E_r\Big|_{i+\frac{1}{2},j}^{n} + \psi_r\Big|_{i+\frac{1}{2},j}^{n} - \frac{\Delta t}{\varepsilon_0\Delta z}\left(H_\varphi\Big|_{i+\frac{1}{2},j+\frac{1}{2}}^{n+\frac{1}{2}} - H_\varphi\Big|_{i+\frac{1}{2},j-\frac{1}{2}}^{n+\frac{1}{2}}\right)\right] \tag{15}$$

where χ_0 is found by evaluating the integral in (9) as

$$\chi_0 = \sum_{q=1}^{13} a_q \left[1 - e^{-(2\pi F_q)\Delta t}\right]. \tag{16}$$

If we follow the same procedure for (5b), the update equation for E_z can easily be obtained:

$$E_z\Big|_{i,j+\frac{1}{2}}^{n+1} = \frac{1}{\varepsilon_\infty + \chi_0 + \frac{\sigma_0\Delta t}{\varepsilon_0}} \times \left[\varepsilon_\infty E_z\Big|_{i,j+\frac{1}{2}}^{n} + \psi_z\Big|_{i,j+\frac{1}{2}}^{n} + \frac{\Delta t}{\varepsilon_0 r_i \Delta r}\left(r_{i+\frac{1}{2}} H_\varphi\Big|_{i+\frac{1}{2},j+\frac{1}{2}}^{n+\frac{1}{2}} - r_{i-\frac{1}{2}} H_\varphi\Big|_{i-\frac{1}{2},j+\frac{1}{2}}^{n+\frac{1}{2}}\right)\right] \tag{17}$$

where ψ_z can be written as

$$\psi_z\Big|_{i,j+\frac{1}{2}}^{n} = E_z|_{i,j+\frac{1}{2}}^{n} \Delta\chi_0 + \sum_{q\,=\,1}^{13} \left[\left(e^{-(2\pi F_q)\Delta t}\right) \psi_{z,q}|_{i,j+\frac{1}{2}}^{n-1}\right]. \tag{18}$$

In the air part, the update equations of classical FDTD can be used. In the soil part, the update equations in (15) and (17) should be used where ψ_r and ψ_z are dependent on the convolution of respective electric fields with susceptibility term and updated recursively with the RC technique. The update equation for H_φ is the same with that of classical FDTD everywhere in the solution domain.

C. Singularity Treatment

To overcome the singularity problem occurring at $r = 0$ in (17), we can solve the integral form of Maxwell's equation [37] derived from Ampere's law for E_z and obtain the following update equation:

$$E_z\Big|_{0,j+\frac{1}{2}}^{n+1} = \frac{\varepsilon_\infty E_z\Big|_{0,j+\frac{1}{2}}^{n} + \psi_z\Big|_{0,j+\frac{1}{2}}^{n} + \frac{4\Delta t}{\varepsilon_0\Delta r} H_\varphi\Big|_{\frac{1}{2},j+\frac{1}{2}}^{n+\frac{1}{2}}}{\varepsilon_\infty + \chi_0 + \frac{\sigma_0\Delta t}{\varepsilon_0}}. \tag{19}$$

D. Absorbing Boundary Condition

The open FDTD boundary domain must be terminated with a proper absorbing boundary condition (ABC). Although one-way wave equation-based ABCs are often used in lightning simulations, they assume a constant phase velocity and their reflection coefficients are functions of the incident angle so that they are successful only under certain conditions [38]. Considering the dispersive nature of Debye medium, we use a convolution perfectly matched layer (CPML) since its implementation is

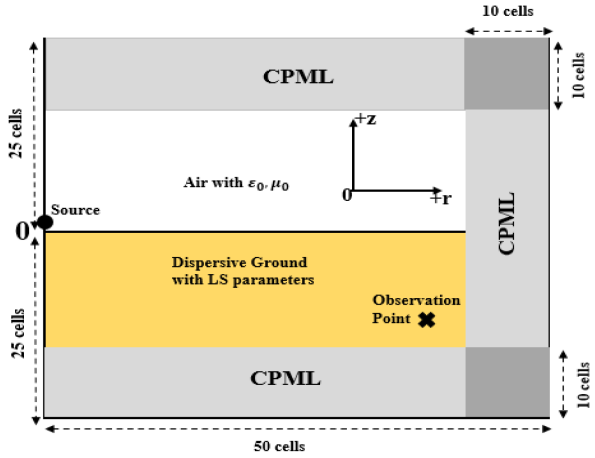

Fig. 1. Test grid of 50×50 cells for measuring the performance of CPML.

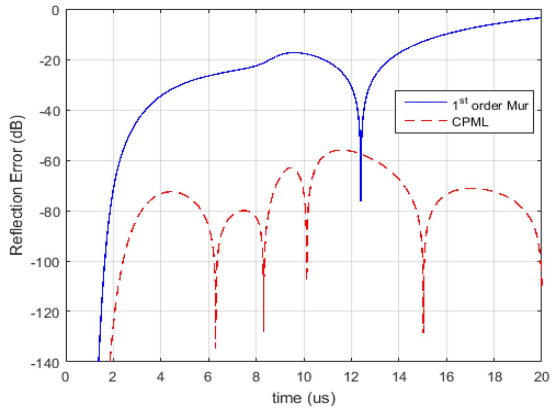

Fig. 2. Reflection error in dB obtained for the CPML and the first order Mur.

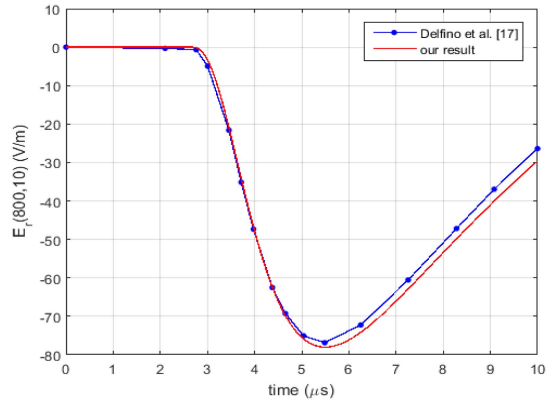

Fig. 3. Comparison of E_r for $p = 1\%$ at a horizontal distance of 800 m and height of 10 m above the ground.

independent of the medium and it is efficient in dispersive media [39]. The update equations of CPML in cylindrical coordinates are constituted using expressions in [29] and [40].

We defined a test grid of 50×50 cells, whose bottom half is filled with dispersive soil of the LS model, as shown in Fig. 1. A 10-cell-thick CPML is defined at the grid edges and a point source is located at the axis of $r = 0$ just over the ground level. The point source, which represents the channel base current of a first return stroke, is defined as the combination of Heidler's functions whose parameters are taken as the same as [37]. We defined the spatial increments Δr and Δz as 5 m, time increment Δt as 5 ns and water percentage of the soil p as 2.59%. The observation point is located two cells away from the bottom corner of the CPML boundary in both directions, namely at the grid point (38, -13).

The CPML performance is assessed by comparing H_φ result with a reference simulation with no boundary reflections. The reflection error relative to the reference simulation is calculated as in [39]. By using trial and error method, the best CPML fit is obtained for the following parameters:

$$\kappa_{max} = 2.45;\ \alpha = 5.5 \times 10^{-6} \tag{20a}$$

$$\sigma_{max} = 0.75\,(m+1)\,/\,(150\pi\Delta r) \tag{20b}$$

where κ_{max} is the maximum mesh scaling parameter at the end of PML region, α is the complex frequency shifting parameter that is especially effective on absorbing evanescent waves at low frequencies, σ_{max} is the maximum conductivity and m is the polynomial scaling order and equals 4. We compare the performance of the CPML with that of first order

Mur's ABC [41]. For the Mur's ABC, the phase velocity in the soil is calculated considering the source center frequency, as suggested in [42]. We take the source frequency as 1 kHz and computed the phase velocity as in [43]. The performance of CPML is much better than that of first-order Mur's ABC, as can be seen in Fig. 2. Its reflection error is 58.99 dB below the Mur's error on average.

E. Verification of the Proposed Computations

We test our computations by comparing the results with Delfino et al. [17] and Sun et al. [29], both of which adopted the LS model for the dispersive ground. We use the same parameters with those in the corresponding papers. Our calculations are successfully verified at both above-ground and underground observation points for the horizontal electric field E_r, as depicted in Figs. 3 and 4, respectively. Fig. 3 compares our above-ground result (10 m above the ground level) with that of Delfino et al. [17] who used inverse Fourier transform to convert their frequency domain results to time domain. The reason of the slight difference between the two results especially after the peak point may be the numerical inverse Fourier transform. Fig. 4 compares our underground result (5 m under the ground level) with that of Sun et al. [29] who compute the fields using FDTD with SARC. It is observed that the two results are perfectly matched so that our results are reliable and can be used for further analysis.

III. Numerical Example

In order to observe the effect of the frequency dependence, the simulations in [37] are repeated. The problem configuration at 50 km is shown in Fig. 5. First, we compare the dispersive ground having the LS parameters with the lossy flat ground

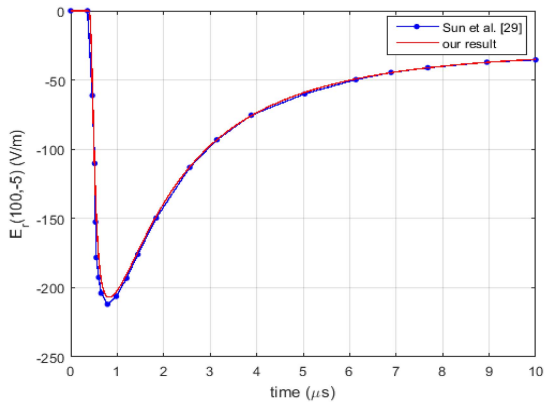

Fig. 4. Comparison of E_r for $p = 5.3\%$ at a horizontal distance of 100 m and depth of 5 m under the ground.

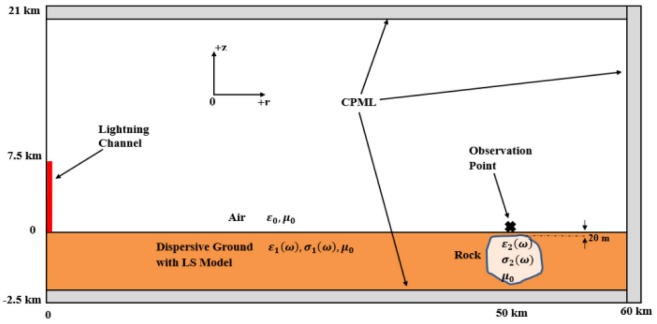

Fig. 5. Problem scenario of the dispersive ground with the dispersive rock formation at 50 km away from the channel.

having constant parameters. Then, we included a rock formation buried in the ground. The results are compared at 500 m, 5 km, and 50 km away from the channel.

The ground is modeled as the multipole Debye medium using the LS parameters as described in Section II-A. The rock is modeled as the single-pole Debye medium, and its parameters are calculated as in [37] and [44]. All other parameters are kept same with [37]; however, we decreased the spatial increment Δr and the time increment Δt to 5 m and 5 ns, respectively, to increase accuracy at 500 m and 5 km simulations and decreased the rock size by 5 at 500 m simulation since it would not fit into the solution domain otherwise. Also, only the *random* shaped rock, whose randomness model details are described in [37], is included in our simulations. The water percentage p is set to 2.59% corresponding to the low-frequency soil resistivity of roughly 1000 Ω·m. It is worth mentioning that *limestone* and *graphite* represents the rocks having very low and very high conductivity, respectively.

A. Results Only for Dispersive Flat Ground Without Rock

Comparison of E_r above the flat ground under subsequent stroke and those of E_z and H_φ under the flat ground under first stroke at 5 km away are shown in Figs. 6 –8, respectively. In these figures, it is seen that the result with the dispersive case has an absolute peak value less than that of the one with the lossy case, and the general waveform of the two curves

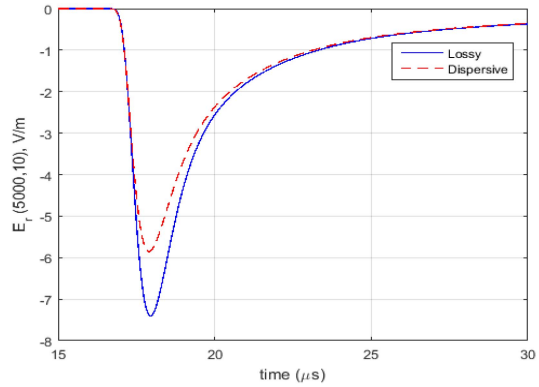

Fig. 6. Comparison of the lossy and the dispersive flat grounds for E_r at 5 km away and 10 m above the ground for subsequent stroke when there is no rock.

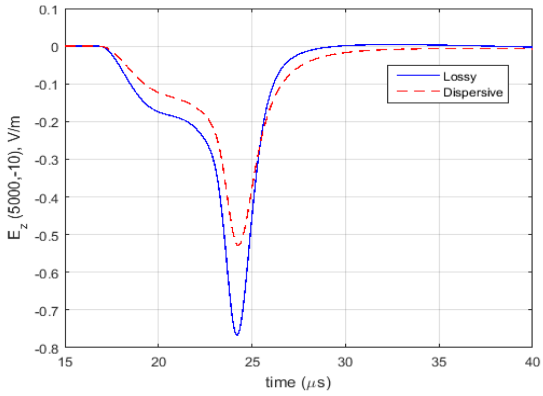

Fig. 7. Comparison of the lossy and the dispersive flat grounds for E_z at 5 km away and 10 m below the ground for first stroke when there is no rock.

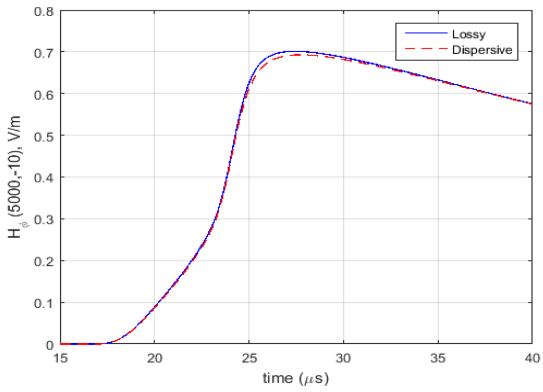

Fig. 8. Comparison of the lossy and the dispersive flat grounds for H_φ at 5 km away and 10 m below the ground for first stroke when there is no rock.

are like each other, which are deductions compatible with the findings of previous research [17], [29]. In fact, these relationships between the two results are preserved at all configurations, namely both stroke types and 500 m, 5 km, 50 km distances, for all the field components. Therefore, to present the results in a compact way, these are evaluated along "No rock" lines in Tables II and III.

TABLE II
RD IN PERCENT BETWEEN LOSSY AND DISPERSIVE RESULTS FOR DIFFERENT CONFIGURATIONS AT 10 M ABOVE THE GROUND

		First Stroke			Subsequent Stroke		
		500 m	5 km	50 km	500 m	5 km	50 km
E_r	No rock	15.26	16.55	15.45	30.83	21.33	19.09
	Limestone	29.78	14.99	9.86	31.48	22.08	11.44
	Graphite	6.81	10.38	8.03	29.75	18.09	11.02
E_z	No rock	0.27	1.89	5.4	1.48	9.17	14.01
	Limestone	0.44	1.64	5	1.48	9.01	13.65
	Graphite	0.22	1.95	5.5	1.48	9.18	14.34
H_φ	No rock	0.49	2.31	5.44	3.08	9.47	14.04
	Limestone	0.56	2.46	5.6	3.11	9.58	14.26
	Graphite	0.41	2.18	5.29	3.06	9.36	13.76

TABLE III
RD IN PERCENT BETWEEN LOSSY AND DISPERSIVE RESULTS FOR DIFFERENT CONFIGURATIONS AT 10 M BELOW THE GROUND

		First Stroke			Subsequent Stroke		
		500 m	5 km	50 km	500 m	5 km	50 km
E_r	No rock	18.56	17.41	15.24	28.95	22.8	18.25
	Limestone	12.53	10.79	10.94	17.34	19.59	12.39
	Graphite	16.15	9.98	4.99	28.71	18.88	7.66
E_z	No rock	33.03	31.64	25.98	47.07	38.93	28.2
	Limestone	61.27	10.32	11.05	61.77	22.35	12.01
	Graphite	55.85	36.8	36	46.65	36.21	33.76
H_φ	No rock	2.65	2.12	2.39	5.44	3.63	7.84
	Limestone	7.44	8.08	14.78	10.02	9.31	16.42
	Graphite	2.53	2.31	2.27	7.51	4.99	6.3

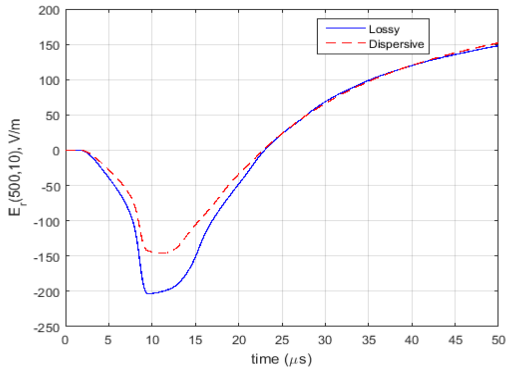

Fig. 9. Comparison of the lossy and the dispersive cases for E_r at 500 m away and 10 m above the ground for the first stroke and the limestone rock.

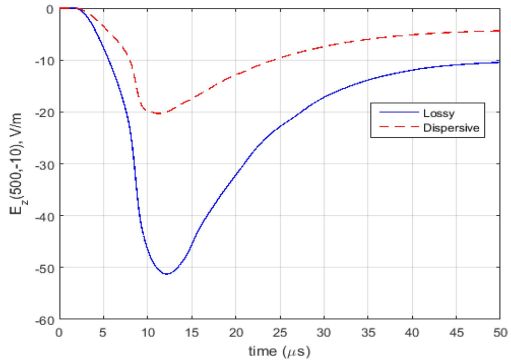

Fig. 10. Comparison of the lossy and the dispersive cases for E_z at 500 m away and 10 m under the ground for the first stroke and the limestone rock.

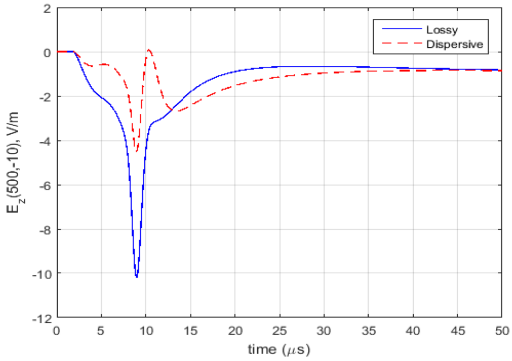

Fig. 11. Comparison of the lossy and the dispersive cases for E_z at 500 m away and 10 m under the ground for the first stroke and the graphite rock.

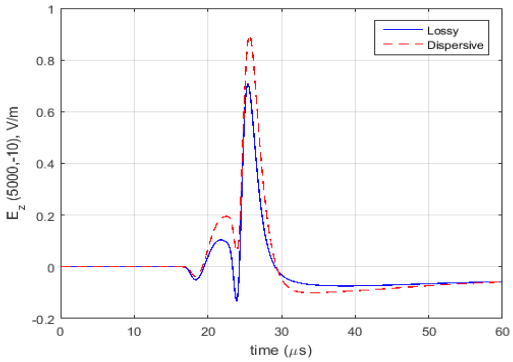

Fig. 12. Comparison of the lossy and the dispersive cases for E_z at 5 km away and 10 m under the ground for the first stroke and the graphite rock.

B. Results of Dispersive Ground With Buried Dispersive Rock

Now, the case of dispersive ground with buried dispersive rock and the case of lossy ground with buried lossy rock (soil and rock with constant parameters) are compared. Some of the comparisons are shown in Figs. 9–14. All the comparisons are not included in this article. Instead, the most salient ones at different distances are shown.

After adding a rock formation inside the ground, we obtain more interesting results than those of the flat ground case. For example, using dispersive parameters decreases the absolute peak values for the low-conductive rock *limestone* whereas they may increase for the high-conductive rock *graphite* in some cases. Also, the difference between the results for dispersive and lossy cases may be very high, as in Fig. 10. Most importantly, the waveforms of the curves look very different in some configurations, as in Fig. 11. The decreases in absolute values of both E_r and E_z, especially the peak values, when the low conductive rock is used are obviously observed in Figs. 9 and 10, respectively. On the other hand, Figs. 12–14 clearly show that almost all the absolute values of E_z under the ground at middle and far ranges (5 km and 50 km), including both global and local

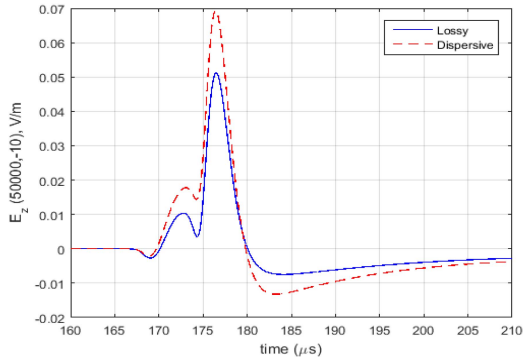

Fig. 13. Comparison of the lossy and the dispersive cases for E_z at 50 km away and 10 m under the ground for the first stroke and the graphite rock.

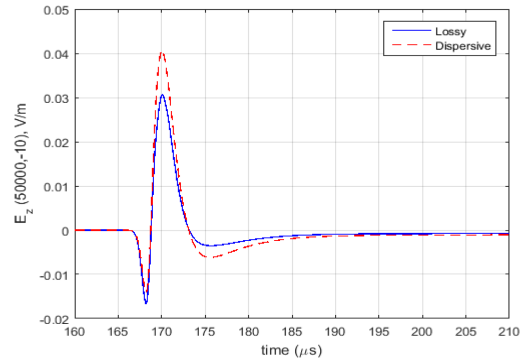

Fig. 14. Comparison of the lossy and dispersive cases for E_z at 50 km away and 10 m under the ground for the subsequent stroke and the graphite rock.

peaks of the field curves, increase when the high conductive rock is adopted; however, this effect is not observed in Fig. 11 where near range values of E_z at 500 m is shown. Considering all the results, it can be inferred that all results including all the field components both for the low conductive limestone and the high conductive graphite show a decrease if dispersive soil model is used. Nonetheless, the only exceptions for this are the underground E_z fields for the high conductive graphite at the middle range 5 km and the far range 50 km because the absolute E_z values under the ground increase at those ranges if the dispersive soil model is used, which can be easily observed in Figs. 12–14.

To quantify the difference between the results, we defined the Relative Difference (RD) in percent as follows:

$$RD \;=\; 100 \times \left(\frac{\max |D_i - L_i|}{\max |L_i|} \right) \tag{21}$$

where D_i and L_i are the values of the dispersive and lossy solutions at each ith data point on the time axis, respectively. The difference between the lossy and the dispersive cases for all configurations are summarized in Tables II and III, respectively, where the influences of different distances, stroke types, and rock types as well as the case without rock are all observed on E_r, E_z, and H_φ.

The results show that there may be a huge difference between the lossy and dispersive cases depending on the configuration. Both the electric fields E_r and E_z are greatly influenced by the frequency-dependence whereas H_φ is influenced less at both above and under the ground. Also, the RD for the E_z is small for the above-ground results whereas the biggest RD values increasing up to 61.77% are obtained for E_z under the ground especially at 500 m away. On the other hand, the most influenced field is the E_r whose RD values are large in all conditions, especially for the subsequent stroke. Although the effect of the horizontal distance cannot be generalized because it depends on the configuration, the fact that the influence of the subsequent stroke is more than that of the first stroke on all the fields is obvious. Also, the rock type does not either influence the fields in the same manner; however, the low conductive rock limestone has more influence on E_r above the ground level and on E_z under the ground, in general.

All the simulations are performed with an i7-4720HQ notebook with 2.6 GHz CPU speed and 16 GB RAM. The most stringent scenario for the 50 km observation point needs 3.63 GB RAM, 11.65 h computation time and 3.30 GB RAM, 10.31 h computation time for the dispersive and lossy cases, respectively.

IV. Conclusion

In this article, the FDTD method combined with the RC technique is applied to directly compute the LEMP for the dispersive ground. Different from other studies utilizing the approximations like the vector fitting, our method includes no approximation in which the dispersive soil parameters are directly employed by treating the ground as a multipole Debye medium using the Longmire and Smith model. Our computations are successfully verified with the results in the literature. In addition, the performances of the CPML ABC over 1st order Mur are shown for the first time in the literature for a source of lightning time dependency. As a numerical example, we included a rock, which is also modeled as Debye medium, inside the ground and conducted simulations at near and far distances at both above and under the ground.

It has been observed that E_z is mainly influenced by the dispersive soil at the observation point under the ground whereas E_r is influenced both above and under the ground for the flat ground case. The same inference can also be made after including a rock inside the ground. The change in H_φ is little compared to the electric fields. In some configurations, more than 60% difference are observed between the simulations with dispersive (frequency-dependent) and lossy (constant electrical parameters) cases. Hence, using constant electrical parameters may lead to incorrect results depending on the conditions and dispersive parameters should be considered in the simulation especially concerning the electric fields E_r and E_z. In future works, computation of electromagnetic fields for different soil conditions, outcrop rocks, and experimental validations can be intended.

References

[1] K. S. Yee, "Numerical solution of initial boundary value problems involving Maxwell's equations in isotropic media," *IEEE Trans. Antennas Propag.*, vol. AP-14, no. 3, pp. 302–307, May 1966.

[2] Y. Baba and V. A. Rakov, "Applications of the FDTD method to lightning electromagnetic pulse and surge simulations," *IEEE Trans. Electromagn. Compat.*, vol. 56, no. 6, pp. 1506–1521, Dec. 2014.

[3] D. Cavka, N. Mora, and F. Rachidi, "A comparison of frequency-dependent soil models: Application to the analysis of grounding systems," *IEEE Trans. Electromagn. Compat.*, vol. 56, no. 1, pp. 177–187, Feb. 2014.

[4] S. Visacro and R. Alipio, "Frequency dependence of soil parameters: Experimental results, predicting formula and influence on the lightning response of grounding electrodes," *IEEE Trans. Power Del.*, vol. 27, no. 2, pp. 927–935, Apr. 2012.

[5] C. Yang and B. Zhou, "Calculation methods of electromagnetic fields very close to lightning," *IEEE Trans. Electromagn. Compat.*, vol. 46, no. 1, pp. 133–141, Feb. 2004.

[6] M. Mokhtari, Z. Abdul-Malek, and C. L. Wooi, "Integration of frequency dependent soil electrical properties in grounding electrode circuit model," *Int. J. Elect. Comput. Eng.*, vol. 6, no. 2, pp. 792–799, Apr. 2016.

[7] R. Alipio and S. Visacro, "Impulse efficiency of grounding electrodes: Effect of frequency-dependent soil parameters," *IEEE Trans. Power Del.*, vol. 29, no. 2, pp. 716–723, Apr. 2014.

[8] F. H. Silveira, S. Visacro, R. Alipio, and A. Conti, "Lightning-induced voltages over lossy ground: The effect of frequency dependence of electrical parameters of soil," *IEEE Trans. Electromagn. Compat.*, vol. 56, no. 5, pp. 1129–1136, Oct. 2014.

[9] S. Visacro and F. H. Silveira, "The impact of the frequency dependence of soil parameters on the lightning performance of transmission lines," *IEEE Trans. Electromagn. Compat.*, vol. 57, no. 3, pp. 434–441, Jun. 2015.

[10] A. Conti, V. C. Oliveira, P. R. Rodrigues, F. H. Silveira, J. L. Silvino, and R. Alipio, "Effect of a lossy dispersive ground on lightning overvoltages transferred to the low-voltage side of a single-phase distribution transformer," *Electric Power Syst. Res.*, vol. 153, pp. 104–110, Dec. 2017.

[11] R. Alipio, D. Conceiçao, A. Conti, K. Yamamoto, R. N. Dias, and S. Visacro, "A comprehensive analysis of the effect of frequency-dependent soil electrical parameters on the lightning response of wind-turbine grounding systems," *Electric Power Syst. Res.*, vol. 175, Oct. 2019, Art. no. 105927.

[12] Q. Zhang, Y. Chen, and W. Hou, "Lightning-induced voltages caused by lighting strike to tall objects considering the effect of frequency dependent soil," *J. Atmos. Sol-Terr. Phy.*, vol. 133, pp. 145–156, Oct. 2015.

[13] M. Akbari, K. Sheshyekani, and M. R. Alemi, "The effect of frequency dependence of soil electrical parameters on the lightning performance of grounding systems," *IEEE Trans. Electromagn. Compat.*, vol. 55, no. 4, pp. 739–746, Aug. 2013.

[14] M. Akbari et al., "Evaluation of lightning electromagnetic fields and their induced voltages on overhead lines considering the frequency dependence of soil electrical parameters," *IEEE Trans. Electromagn. Compat.*, vol. 55, no. 6, pp. 1210–1219, Dec. 2013.

[15] K. Sheshyekani and M. Akbari, "Evaluation of lightning-induced voltages on multiconductor overhead lines located above a lossy dispersive ground," *IEEE Trans. Power Del.,* vol. 29, no. 2, pp. 683–690, Apr. 2014.

[16] J. Paknahad, K. Sheshyekani, F. Rachidi, M. Paolone, and A. Mimouni, "Evaluation of lightning-induced currents on cables buried in a lossy dispersive ground," *IEEE Trans. Electromagn. Compat.*, vol. 56, no. 6, pp. 1522–1229, Dec. 2014.

[17] F. Delfino, R. Procopio, M. Rossi, and F. Rachidi, "Influence of frequency-dependent soil electrical parameters on the evaluation of lightning electromagnetic fields in air and underground," *J. Geophys. Res.*, vol. 114, no. D11, Jun. 2009.

[18] Q. Zhang, T. Ji, and W. Hou, "Effect of frequency-dependent soil on the propagation of electromagnetic fields radiated by subsequent lightning strike to tall objects," *IEEE Trans. Electromagn. Compat.*, vol. 57, no. 1, pp. 112–120, Feb. 2015.

[19] Q. Li et al., "On the influence of the soil stratification and frequency-dependent parameters on lightning electromagnetic fields," *Electric Power Syst. Res.*, vol. 178, Jan. 2020, Art. no. 106047.

[20] C. F. Barbosa, J. O. S. Paulino, and W. d. C. Boaventura, "A time-domain method for the horizontal electric field calculation at the surface of two-layer earth due to lightning," *IEEE Trans. Electromagn. Compat.*, vol. 55, no. 2, pp. 371–377, Apr. 2013.

[21] C. F. Barbosa and J. O. S. Paulino, "On time-domain expressions for calculating the horizontal electric field from lightning," *IEEE Trans. Electromagn. Compat.*, vol. 61, no. 2, pp. 434–439, Apr. 2019.

[22] J. Wu, B. Zhang, J. He, and R. Zeng, "A comprehensive approach for transient performance of grounding system in the time domain," *IEEE Trans. Electromagn. Compat.*, vol. 57, no. 2, pp. 250–256, Apr. 2015.

[23] S. Sekioka, "Frequency and current-dependent grounding resistance model for lightning surge analysis," *IEEE Trans. Electromagn. Compat.*, vol. 61, no. 2, pp. 419–425, Apr. 2019.

[24] R. Alipio and S. Visacro, "Time-domain analysis of frequency-dependent electrical parameters of soil," *IEEE Trans. Electromagn. Compat.*, vol. 59, no. 3, pp. 873–878, Jun. 2017.

[25] H. Chen and Y. Du, "Lightning grounding grid model considering both the frequency-dependent behavior and ionization phenomenon," *IEEE Trans. Electromagn. Compat.*, vol. 61, no. 1, pp. 157–165, Feb. 2019.

[26] M. Moradi, "Analysis of transient performance of grounding system considering frequency-dependent soil parameters and ionization," *IEEE Trans. Electromagn. Compat.*, vol. 62, no. 3, pp. 785–797, Jun. 2020.

[27] D. Kuklin, "Extension of thin wire techniques in the FDTD method for Debye media," *Prog. Electromagn. Res. M*, vol. 51, pp. 9–17, Oct. 2016.

[28] R. M. S. Oliveira, D. M. Fujiyoshi, R. C. F. Araujo, J. A. S. Nascimento, and L. F. P. Carvalho, "Finite-difference modeling of dispersive soils validated via experimental evaluation of transient grounding signals," *J. Electrostatics*, vol. 87, pp. 263–275, Jun. 2017.

[29] Z. Sun, L. Shi, Y. Zhou, B. Yang, and W. Jiang, "FDTD evaluation of LEMP considering the lossy dispersive ground," *Appl. Comput. Electromagn. Soc. J.*, vol. 33, no. 1, pp. 7–14, Jan. 2018.

[30] M. E. M. Rizk, S. Abulanwar, A. Ghanem, and M. Lehtonen, "Computation of lightning-induced voltages considering ground impedance of multi-conductor line for lossy dispersive soil," *IEEE Trans. Power Del.*, vol. 37, no. 4, pp. 2464–2473, Aug. 2022.

[31] C. L. Longmire and K. S. Smith, "A universal impedance for soils," Defense Nucl. Agency, Santa Barbara, CA, USA, Topical Report for Period, 1 Jul.–30 Sep. 1975.

[32] F. Krewer, F. Morgan, and M. O'Halloran, "Development of accurate multi-pole Debye functions for electromagnetic tissue modelling using a genetic algorithm," *Prog. Electromagn. Res. Lett.*, vol. 43, pp. 137–147, Oct. 2013.

[33] R. Luebbers, F. P. Hunsberger, K. S. Kunz, R. B. Standler, and M. Schneider, "A frequency-dependent finite-difference time-domain formulation for dispersive materials," *IEEE Trans. Electromagn. Compat.*, vol. 32, no. 3, pp. 222–227, Aug. 1990.

[34] F. L. Teixeira, "Time-domain finite-difference and finite-element methods for Maxwell equations in complex media," *IEEE Trans. Antennas Propag.*, vol. 56, no. 8, pp. 2150–2166, Aug. 2008.

[35] R. J. Luebbers and F. Hunsberger, "FDTD for Nth-order dispersive media," *IEEE Trans. Antennas Propag.*, vol. 40, no. 11, pp. 1297–1301, Nov. 1992.

[36] S. Aksoy, "An alternative algorithm for both narrow and wide band Lorentzian dispersive materials modeling in the finite difference time domain method," *IEEE Trans. Microw. Theory Techn.*, vol. 55, no. 4, pp. 703–708, Apr. 2007.

[37] O. Kurnaz and S. Aksoy, "Electromagnetic fields radiated by lightning return stroke over lossy ground with rock formation," *IEEE Trans. Electromagn. Compat.*, vol. 63, no. 5, pp. 1444–1451, Oct. 2021.

[38] U. S. Inan and R. A. Marshall, *Numerical Electromagnetics: The FDTD Method*. New York, NY, USA: Cambridge Univ. Press, 2011, pp. 174–199.

[39] J. A. Roden and S. D. Gedney, "Convolution PML (CPML): An efficient FDTD implementation of the CFS-PML for arbitrary media," *Microw. Opt. Technol. Lett.*, vol. 27, no. 5, pp. 334–339, Dec. 2000.

[40] Y.-G. Wang, B. Chen, H.-L. Chen, Y. Yi, and X.-L. Kong, "One-step leapfrog ADI-FDTD method in 3-D cylindrical grids with a CPML implementation," *IEEE Antennas Wireless Propag. Lett.*, vol. 13, pp. 714–717, Apr. 2014.

[41] A. Mimouni, F. Rachidi, and Z. Azzouz, "Electromagnetic environment in the immediate vicinity of a lightning return stroke," *J. Lightning Res.*, vol. 2, pp. 64–75, 2007.

[42] Y. Yu and J. J. Simpson, "A magnetic field-independent absorbing boundary condition for magnetized cold plasma," *IEEE Antennas Wireless Propag. Lett.*, vol. 10, pp. 294–297, Apr. 2011.

[43] C. A. Balanis, *Advanced Engineering Electromagnetics*, 2nd ed. Hoboken, NJ, USA: Wiley, 2012, p. 142.

[44] Z. He, K. Huang, C. Guo, Z. Jin, and C. Hou, "A debye dispersion model of a two-layered material," *AIP Adv.*, vol. 9, Apr. 2019, Art. no. 045321.